Electrochemical Oxidation of Methanol with Ru/Pd, Ru/Pt, and Ru/Au Heterobimetallic Complexes

Gilbert J. Matare, Mark E. Tess, Ying Yang, Khalil A. Abboud, and Lisa McElwee-White*

Department of Chemistry and Center for Catalysis, University of Florida, Gainesville, Florida 32611

Received August 6, 2001

The heterobimetallic complexes $CpRu(PPh_3)(\mu\text{-}Cl)(\mu\text{-}dppm)PdCl_2$ (**1**) [dppm = bis(diphenylphosphino)methane], $CpRu(PPh_3)Cl(\mu\text{-}dppm)AuCl$ (**2**), and $CpRu(PPh_3)(\mu\text{-}Cl)(\mu\text{-}dppm)PtCl_2$ (**3**) were synthesized by the reaction of $CpRu(PPh_3)Cl(\eta^1\text{-}dppm)$ (**4**) with $Pd(COD)Cl_2$, $AuPPh_3Cl$, and $Pt(COD)Cl_2$, respectively. Compounds **1** and **2** were characterized by X-ray crystallography. Electrochemical oxidation of CH_3OH in the presence of **1**, **2**, or **3** leads to considerable enhancement of the oxidative currents and formation of the organic products $CH_2(OCH_3)_2$ and $HCOOCH_3$. Addition of water increases both the current and the proportion of the more highly oxidized product, $HCOOCH_3$. Current efficiencies obtained with heterobinuclear complexes **1**−**3** were significantly higher than those obtained using the model compound $CpRuCl(\eta^2\text{-}dppm)$ (**5**) as catalyst.

Introduction

Recent efforts toward the development of electrooxidation catalysts for direct methanol fuel cells have included the incorporation of a second metal to improve the performance of Pt anodes. In addition to the commonly utilized Pt/Ru systems,[1−7] other electrode materials including PtSn,[8−10] PtRe,[10] PtRuOs,[11] and PtRuOsIr[12] have been investigated. Binary Pt/Ru alloys are among the most active, exhibiting lower overpotentials and less surface poisoning than pure Pt anodes. Many experiments have addressed the mechanism of oxidation, kinetics, bulk composition, and the nature of their active sites.[1,12−16] Earlier studies from Watanabe[17] and others[5,18] suggest that the Pt surface is the site of methanol binding and dehydrogenation. The Ru site is implicated in the removal of Pt-adsorbed CO, converting it into CO_2 through intermediate Ru oxo species. These postulates correlate to behavior of discrete species in homogeneous solution since C−H bond rupture has been demonstrated in mononuclear organometallic Pt(II) complexes[19−23] and Ru oxo complexes are well-known oxidants of alcohols.[24−29]

Homogeneous catalysis with well-defined heterobimetallic systems has been a topic of interest due in part to the potential to explore the cooperative interaction of the two metals as well as the possibility for each metal center to perform a separate and distinctive task.[30−38] Recently, we reported the electrochemical

(1) Gasteiger, H. A.; Markovic, N.; Ross, P. N.; Cairns, E. J. *J. Phys. Chem.* **1993**, *97*, 12020−12029.
(2) Wasmus, S.; Kuver, A. *J. Electroanal. Chem.* **1999**, *461*, 14−31.
(3) Gasteiger, H. A.; Markovic, N. M.; Ross, P. N. *J. Phys. Chem.* **1995**, *99*, 8290−8301.
(4) Leger, J. M.; Lamy, C. *Ber. Bunsen-Ges.* **1990**, *94*, 1021−1025.
(5) Goodenough, J. B.; Hamnett, A.; Kennedy, B. J.; Manoharan, R.; Weeks, S. A. *J. Electroanal. Chem. Interfacial Electrochem.* **1988**, *240*, 133−145.
(6) Swathirajan, S.; Mikhail, Y. M. *J. Electrochem. Soc.* **1991**, *138*, 1321−1326.
(7) Reddington, E.; Sapienza, A.; Gurau, B.; Viswanathan, R.; Sarangapani, S.; Smotkin, E. S.; Mallouk, T. E. *Science* **1998**, *280*, 1735−1737.
(8) Wang, K.; Gasteiger, H. A.; Markovic, N. M.; Ross, P. N. *Electrochim. Acta* **1996**, *41*, 2587−2593.
(9) Katayama, A. *J. Phys. Chem.* **1980**, *84*, 376−381.
(10) Cathro, K. J. *J. Electrochem. Soc.* **1969**, *116*, 1608−1611.
(11) Ley, K. L.; Liu, R. X.; Pu, C.; Fan, Q. B.; Leyarovska, N.; Segre, C.; Smotkin, E. S. *J. Electrochem. Soc.* **1997**, *144*, 1543−1548.
(12) Gurau, B.; Viswanathan, R.; Liu, R. X.; Lafrenz, T. J.; Ley, K. L.; Smotkin, E. S.; Reddington, E.; Sapienza, A.; Chan, B. C.; Mallouk, T. E.; Sarangapani, S. *J. Phys. Chem. B* **1998**, *102*, 9997−10003.
(13) Rolison, D. R.; Hagans, P. L.; Swider, K. E.; Long, J. W. *Langmuir* **1999**, *15*, 774−779.
(14) Kabbabi, A.; Faure, R.; Durand, R.; Beden, B.; Hahn, F.; Leger, J. M.; Lamy, C. *J. Electroanal. Chem.* **1998**, *444*, 41−53.
(15) Iwasita, T.; Hoster, H.; John-Anacker, A.; Lin, W. F.; Vielstich, W. *Langmuir* **2000**, *16*, 522−529.
(16) Parsons, R.; VanderNoot, T. *J. Electroanal. Chem.* **1988**, *257*, 9−45.
(17) Watanabe, M.; Motoo, S. *J. Electroanal. Chem.* **1975**, *60*, 276−283.
(18) Hamnett, A.; Kennedy, B. J.; Wagner, F. E. *J. Catal.* **1990**, *124*, 30−40.
(19) Stahl, S. S.; Labinger, J. A.; Bercaw, J. E. *J. Am. Chem. Soc.* **1996**, *118*, 5961−5976.
(20) Stahl, S. S.; Labinger, J. A.; Bercaw, J. E. *Angew. Chem., Int. Ed.* **1998**, *37*, 2181−2192.
(21) Holtcamp, M. W.; Henling, L. M.; Day, M. W.; Labinger, J. A.; Bercaw, J. E. *Inorg. Chim. Acta* **1998**, *270*, 467−478.
(22) Holtcamp, M. W.; Labinger, J. A.; Bercaw, J. E. *J. Am. Chem. Soc.* **1997**, *119*, 848−849.
(23) Labinger, J. A.; Herring, A. M.; Lyon, D. K.; Luinstra, G. A.; Bercaw, J. E.; Horvath, I. T.; Eller, K. *Organometallics* **1993**, *12*, 895−905.
(24) Wong, K. Y.; Che, C. M.; Anson, F. C. *Inorg. Chem.* **1987**, *26*, 737−741.
(25) Roecker, L.; Meyer, T. J. *J. Am. Chem. Soc.* **1986**, *108*, 4066−4073.
(26) Roecker, L.; Meyer, T. J. *J. Am. Chem. Soc.* **1987**, *109*, 746−754.
(27) Thompson, M. S.; Meyer, T. J. *J. Am. Chem. Soc.* **1982**, *104*, 4106−4115.
(28) Wong, K. Y.; Yam, V. W.; Lee, W. W. *Electrochim. Acta* **1992**, *37*, 2645−2650.
(29) Griffith, W. P. *Chem. Soc. Rev.* **1992**, *21*, 179−185.
(30) Adams, R. D.; Barnard, T. S. *Organometallics* **1998**, *17*, 2885−2890.
(31) Bruce, M. I. *J. Organomet. Chem.* **1983**, *242*, 147−204.
(32) Balch, A. L. In *Reactivity of Metal−Metal Bonds*; Chisholm, M., Ed.; 1981; ACS Symposium Series No. 155; pp 167-185.

10.1021/om010706h CCC: $22.00
Publication on Web 01/15/2002

Scheme 1

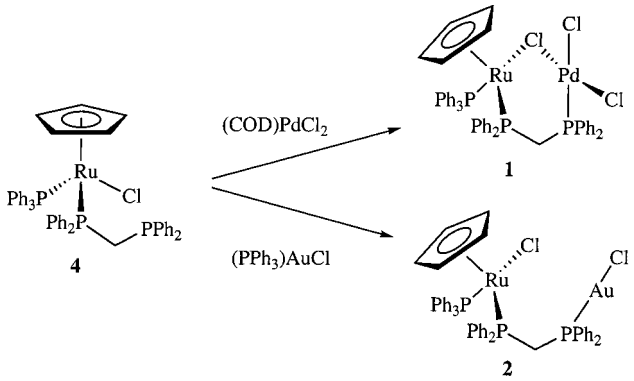

oxidation of methanol catalyzed by the heterobimetallic complex $CpRu(PPh_3)(\mu\text{-}Cl)(\mu\text{-}dppm)PtCl_2$ (**3**).[39] In this work, we report the synthesis, electrochemistry, and electrocatalytic activity of the related heterobimetallic complexes $CpRu(PPh_3)(\mu\text{-}Cl)(\mu\text{-}dppm)PdCl_2$ (**1**) and $[CpRu(PPh_3)Cl(\mu\text{-}dppm)AuCl$ (**2**). Further experiments on the catalytic behavior of **3** are also reported herein.

Results and Discussion

Synthesis of Heterobimetallic Complexes. The Ru/Pd complex **1** was prepared as a red air stable powder in 71% yield from the reaction of $CpRu(PPh_3)$-$Cl(\eta^1\text{-}dppm)$ (**4**) with $(COD)PdCl_2$ at room temperature (Scheme 1). Unlike its platinum analogue **3**,[39,40] solutions of **1** do not show signs of decomposition even when exposed to air for weeks. The $^{31}P\{^1H\}$ NMR spectrum of **1** exhibits the expected three resonances. The Ru-bound phosphorus signals appear as a doublet of doublets at 52.2 ppm and a doublet at 37.5 ppm. The upfield resonance at 19.7 ppm is assigned to the Pd-bound phosphorus. Treatment of **4** with $AuPPh_3Cl$ affords the orange heterobimetallic complex **2** in 66% yield. The $^{31}P\{^1H\}$ NMR data for **2** are consistent with the resonances observed for the Ru/Pd catalyst **1**. The Ru-bound phosphorus atoms appear at 42.8 and 36.3 ppm as a doublet and a doublet of doublets, respectively. A doublet at 20.8 ppm is assigned to the Au-bound phosphorus atom. In the ^1H NMR spectrum, the methylene protons of the bridging ligands of **1** are observed as a multiplet at approximately 2.6 ppm as a result of coupling to the adjacent phosphorus atoms. Similar coupling is observed in **2**, but the chemical shifts of the diastereotopic methylene protons are significantly different.

X-ray Crystal Structures of Complexes 1 and 2. Complex **1** exhibits a bridging chloride (Figure 1), as does its structurally similar Ru/Pt analogue **3**.[39] The six central atoms in **1** (Pd, P1, C6, P2, Ru, and the μ-Cl) form a distorted six-membered ring, in which the Cp ligand occupies an apical position. In contrast, as seen in Figure 2, complex **2** exhibits no interaction between the Ru and Au centers beyond what could be transmitted via through-bond interactions involving the dppm ligand. In both complexes, the cyclopentadienyl ligands are coordinated to the Ru centers in an η^5 mode, resulting in a pseudotetrahedral geometry typical of a piano stool conformation. The bond lengths and bond angles of the structures are standard, with the expected square planar geometry at Pd and linear configuration at Au.

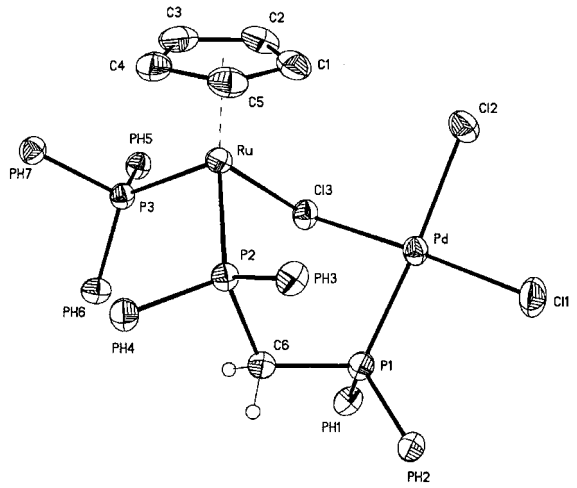

Figure 1. Thermal ellipsoids drawing of the molecular structure of $CpRuPPh_3(\mu\text{-}Cl)(\mu\text{-}dppm)PdCl_2$ (**1**). Thermal ellipsoids are plotted at 50% probability. Phenyl rings and most hydrogen atoms are omitted for clarity.

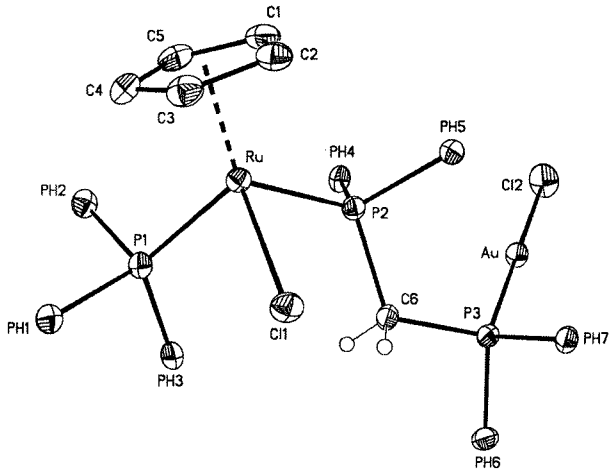

Figure 2. Thermal ellipsoids drawing of the molecular structure of $CpRuPPh_3Cl(\mu\text{-}dppm)AuCl$ **(2)**. Thermal ellipsoids are plotted at 50% probability. Phenyl rings and most hydrogen atoms are omitted for clarity.

Cyclic Voltammetry of Complexes 1−5. Cyclic voltammetry of the Ru/Pd system **1** in DCE/TBAT (DCE = 1,2-dichloroethane, TBAT = tetrabutylammonium trifluoromethanesulfonate) exhibits irreversible couples at 1.29 and 1.45 V vs NHE (Figure 3). The wave at 1.29 V is assigned to the Ru(II/III) couple. This wave is shifted about 160 mV positive compared to that of the Ru/Pt complex **3**, which exhibits a reversible couple at 1.13 V. The shift is consistent with electron donation through the Cl bridge to the more electron-deficient Pd

(33) McCollum, D. G.; Bosnich, B. *Inorg. Chim. Acta* **1998**, *270*, 13−19.
(34) Shapley, P. A.; Zhang, N. J.; Allen, J. L.; Pool, D. H.; Liang, H. C. *J. Am. Chem. Soc.* **2000**, *122*, 1079−1091.
(35) Kalck, P.; Wheatley, N. *Chem. Rev.* **1999**, *99*, 3379−3419.
(36) Baranger, A. M.; Bergman, R. G. *J. Am. Chem. Soc.* **1994**, *116*, 3822−3835.
(37) Beuken, E.; Feringa, B. L. *Tetrahedron* **1998**, *54*, 12985−13011.
(38) Farr, J. P.; Olmstead, M. M.; Wood, F. E.; Balch, A. L. *J. Am. Chem. Soc.* **1983**, *105*, 792−798.
(39) Tess, M. E.; Hill, P. L.; Torraca, K. E.; Kerr, M. E.; Abboud, K. A.; McElwee-White, L. *Inorg. Chem.* **2000**, *39*, 3942−3944.
(40) Orth, S. D.; Terry, M. R.; Abboud, K. A.; Dodson, B.; McElwee-White, L. *Inorg. Chem.* **1996**, *35*, 916−922.

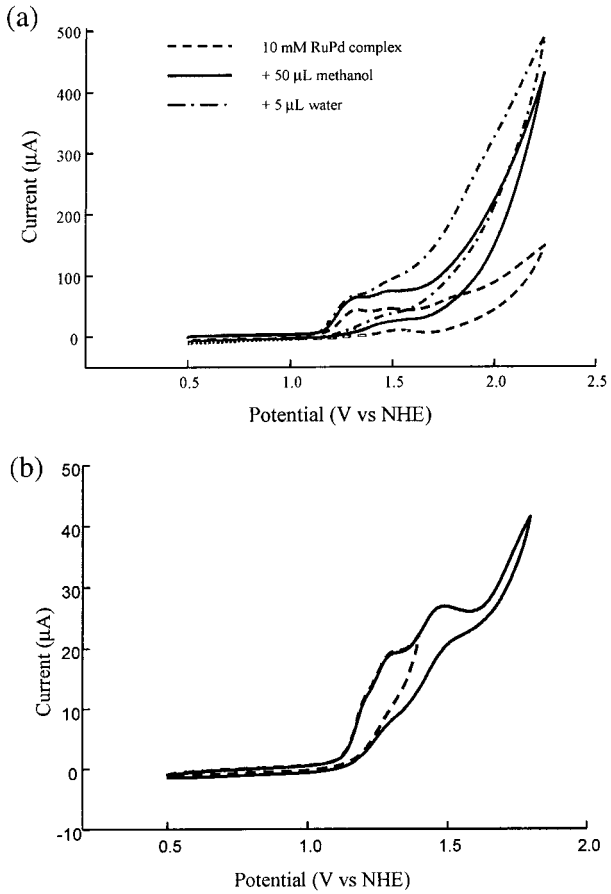

Figure 3. Cyclic voltammograms of **1** under nitrogen in 2.5 mL of DCE/0.7 M TBAT; glassy carbon working electrode; Ag/Ag^+ reference electrode; 50 mV/s: (a) solutions as specified in figure; (b) 10 mM **1**; 5 mV/s; (—) switching potential 1.8 V; (- - -) switching potential 1.3 V.

center of **1** (the first oxidation wave of the model compound $PdCl_2(\eta^2$-dppm) is approximately 200 mV positive of its Pt analogue). The irreversible wave at 1.45 V is assigned to the Pd(II/IV) oxidation based on comparisons with the cyclic voltammogram of $PdCl_2(\eta^2$-dppm). The formal oxidation wave potentials for the bimetallic complexes **1**−**3** as well as the mononuclear Ru complexes **4** and **5** are summarized in Table 4.

The Ru/Au complex **2** exhibits a reversible couple at 0.86 V and a quasireversible couple at 1.40 V vs NHE in DCE/TBAT (Figure 4). The reversibility of the wave at 0.86 V is not affected by oxidation in the presence of methanol at potentials up to 1.5 V (Figure 4b). The wave at 0.86 V is assigned to the Ru(II/III) couple, while the wave at 1.40 V is assigned to the Au(I/III) oxidation. This wave is similar to that of the starting material, $Au(PPh_3)Cl$, which has been reported to oxidize at 1.68 V vs NHE in CH_2Cl_2.[41] The Ru(II/III) wave of the mononuclear compound $CpRu(PPh_3)Cl(\eta^1$-dppm) (**4**) is observed at 0.56 V.[40] Overall, the first two redox potentials of **2** more closely resemble their mononuclear model compounds than do the first two redox potentials of **1**. This is consistent with the crystal structure data, which suggest that interactions between the metal centers of **2** are likely to be minimal, while coupling of the metals via the μ-Cl bridge of **1** is more substantial. We have also examined the cyclic voltammetric behavior of the mononuclear Ru model complex $CpRuCl(\eta^2$-dppm) (**5**) (Figure 5). The Ru(II/III) couple of **5** occurs at 0.61 V, while the Ru(III/IV) couple is observed at 1.38 V.

Catalytic Electrooxidation of Methanol By Complexes 1−3. The cyclic voltammogram of the Ru/Pd complex $CpRu(PPh_3)(\mu$-Cl)(μ-dppm)$PdCl_2$ (**1**) after addition of methanol (Figure 3a) shows a minimal current increase at the Ru(II/III) couple followed by a dramatic increase at the Pd(II/IV) wave. In contrast, methanol oxidation with the Ru/Au complex $CpRu(PPh_3)Cl(\mu$-dppm)AuCl (**2**) occurs at the Ru(III/IV) wave, which is similar to alcohol oxidation with simple mononuclear Ru complexes.[24,42−45] Cyclic voltammograms of the model monometallic Ru complex **5** under the same conditions as the bimetallic compounds exhibit considerable increases in the voltammetric current in the presence of methanol. However, the onset of oxidation occurs at potentials far more positive relative to the Ru(III/IV) wave of the bimetallic complexes. Electrochemical oxidation of methanol in the presence of **1** or **2** leads to considerable enhancement of the oxidative currents. Methanol oxidation with **2** occurs at a potential more positive than with **1**. In the absence of methanol, no anodic activity is observed. Addition of 5 μL of water to the samples results in further current increases.

Differences among the behavior of **1**, **2**, and **3** can be seen in the evolution of product distributions shown in Tables 5 and 6, which present the average product ratios of dimethyl acetal to methyl formate formed during bulk electrolysis of dry and wet methanol. The presence of water consistently shifts the product ratios toward the four-electron oxidation product, $HCOOCH_3$. This trend is reflected by all the complexes and can be seen both in the initial product ratios for wet vs dry samples and in the tendency toward production of more methyl formate in the dry samples as the reaction progresses. The time evolution of product ratios in the dry samples presumably arises from water that is generated in situ during the condensation of formaldehyde[46] and formic acid with excess methanol. This behavior is consistent with the catalytic performance of complex **3** observed previously.[39]

The potential for bulk electrolyses (1.7 V vs NHE) was chosen during earlier studies on Ru/Pt complex **3**, which exhibits its rise in catalytic current coincident with the Pt(II/IV) wave at that potential.[39] For comparison purposes, bulk electrolyses with complexes **1**, **2**, and **5** were performed at the same potential. Thus, oxidations with Ru/Pd complex **1** were performed between the Pd(II/IV) and Ru(III/IV) waves, while Ru/Au compound **3** was electrolyzed between the Au(I/III) and Ru(III/IV) waves. The Ru complex **5** was oxidized at a potential somewhat more positive than the Ru(III/IV) couple. Thus, for all of the bimetallic complexes, oxidation was positive of both the Ru(II/III) couple and the first oxidative wave for the second metal. Only in model compound **5** had

(41) Attar, S.; Nelson, J. H.; Bearden, W. H.; Alcock, N. W.; Solujic, L.; Milosavljevic, E. B. *Polyhedron* **1991**, *10*, 1939−1949.
(42) Gagné, R. R.; Marks, D. N. *Inorg. Chem.* **1984**, *23*, 65−74.
(43) Navarro, M.; De Giovani, W. F.; Romero, J. R. *J. Mol. Catal. A: Chem.* **1998**, *135*, 249−256.
(44) Lima, E. C.; Fenga, P. G.; Romero, J. R.; De Giovani, W. F. *Polyhedron* **1998**, *17*, 313−318.
(45) Raven, S. J.; Meyer, T. J. *Inorg. Chem.* **1988**, *27*, 4478−4483.
(46) Wasmus, S.; Wang, J. T.; Savinell, R. F. *J. Electrochem. Soc.* **1995**, *142*, 3825−3833.

Table 1. Selected Bond Distances (Å) and Angles (deg) for Complex 1

Pd−Cl1	2.2842(8)	Pd−P1	2.2332(8)	Pd−Cl2	2.3773(8)
Pd−Cl3	2.3256(7)	Ru−P2	2.2979(7)	Ru−P3	2.3347(7)
Ru−Cl3	2.4403(7)				
P1−C6−P2	119.74(15)	P1−Pd−Cl1	91.09(3)	P1−Pd−Cl3	86.50(3)
C13−Pd−Cl2	90.11(3)	Cl1−Pd−Cl3	174.98(3)	Cl1−Pd−Cl2	92.44(3)
Pd−Cl3−Ru	106.76(3)	P2−Ru−Cl3	89.36(2)	P3−Ru−Cl3	89.13(2)
		C6−P1−Pd	113.70(9)		

Table 2. Selected Bond Distances (Å) and Angles (deg) for Complex 2

Au−Cl2	2.2860(13)	Au−P3	2.2288(12)	Ru−P1	2.3165(12)
Ru−Cl1	2.4598(11)	Ru−P2	2.2946(11)		
P3−C6−P2	118.5(5)	P1−Ru−P2	98.36(4)	C6−P2−Ru	116.48(14)
P1−Ru−Cl1	92.65(4)	C6−P2−Au	115.32(15)	P2−Ru−Cl1	88.95(4)
				P3−Au−Cl2	1179.36(5)

Table 3. Crystal Data and Structure Refinement for Complexes 1 and 2

formula	$C_{54}H_{54}Cl_9P_3PdRu$	$C_{49.50}H_{45}AuCl_5P_3Ru$
molecular weight	1322.40	1208.05
cryst syst	monoclinic	triclinic
space group	$P2(1)/n$	$P\bar{1}$
a (Å)	13.7019(8)	11.1888(5)
b (Å)	22.763(1)	13.5263(6)
c (Å)	18.517(1)	15.4678(7)
α (deg)	90	94.690(1)
β (deg)	107.398(1)	90.562(1)
γ (deg)	90	100.561(1)
volume (Å^3)	5511.1(6)	2292.9(1)
Z	4	2
T (K)	173(2)	173(2)
λ (Å)	0.71073	0.71073
σ_{calcd} (Mg/m^3)	1.594	1.750
μ (mm^{-1})	1.160	3.956
F_{000}	2664	1190
cryst size (mm^3)	0.19 × 0.21 × 0.32	0.23 × 0.20 × 0.10
θ range (deg)	1.79 to 27.50	1.85 to 27.50
hkl limits	$-12 \le h \le 17$, $-29 \le k \le 29$, $-24 \le l \le 24$	$-14 \le h \le 14$, $-17 \le k \le 17$, $-20 \le l \le 10$
no. reflns collected	39 100	15 922
no. ind reflns	12 610 [R(int) = 0.0279]	10 266 [R(int) = 0.0379]
no data/restraints/params	12 610/0/666	10 266/0/551
GOF	1.108	0.971
$R(F_o)^a$	0.0346($F>2\sigma(F)$)	0.0375($F>2\sigma(F)$)
$wR(F_o^2)^b$	0.0839	0.0933
largest diff peak/hole (e.Å^{-3})	0.777/−0.902	1.396/−1.431

[a] $R1 = \sum(||F_o| - |F_d||)/\sum|F_o|$. [b] $wR2 = [\sum[w(F_o^2 - F_c^2)^2]/\sum w[F_o]^2]^{1/2}$[$F>2\sigma(F)$].

Table 4. Formal Potentials for Complexes 1−5

complex	couple	$E_{1/2}$ (V)[a]	couple	$E_{1/2}$ (V)[a]
1	Ru(II/III)	1.29[b]	Pd(II/IV)	1.45[b]
2	Ru(II/III)	0.86	Au(I/III)	1.40[b]
3	Ru(II/III)	1.13[c]	Pt(II/IV)	1.78[b,c]
4	Ru(II/III)	0.56[c]		
5	Ru(II/III)	0.61		

[a] All potentials obtained in DCE/TBAT and reported vs NHE. [b] Irreversible wave, E_{pa} reported. [c] Performed in CH_2Cl_2/TBAH as described in ref 40.

Ru reached the Ru(IV) oxidation state. The difference in the identity and the oxidation state of the second metal appears to be reflected in the product ratios of the methanol oxidation products. At early stages of the reaction, all three bimetallic complexes afford higher proportions of dimethyl acetal; however, in oxidation of dry samples with Ru/Pt complex **3** the acetal continues to predominate even at later stages of the reaction

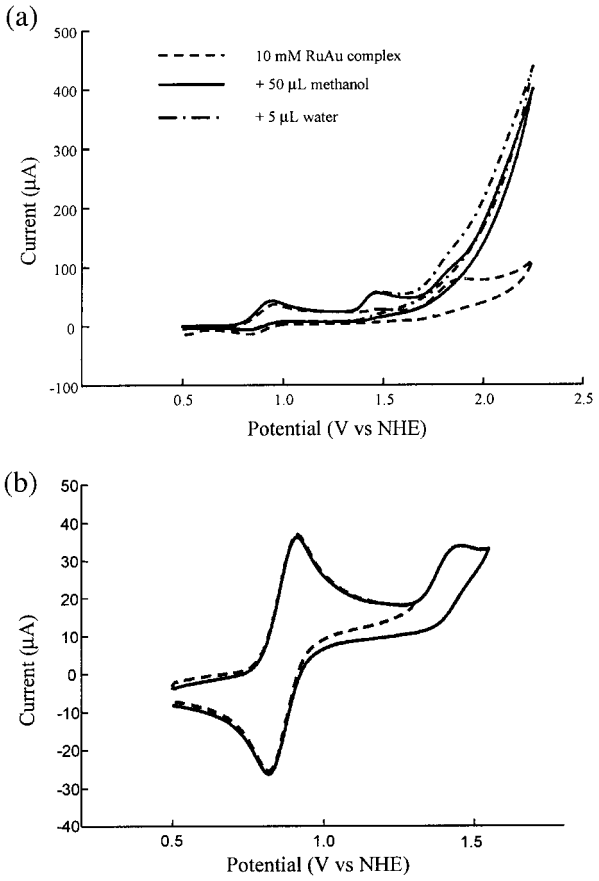

Figure 4. Cyclic voltammograms of **2** under nitrogen in 2.5 mL of DCE/0.7 M TBAT; glassy carbon working electrode; Ag/Ag^+ reference electrode: (a) solutions as specified in figure; 50 mV/s; (b) 10 mM **2** plus 50 μL of methanol; 50 mV/s; (—) switching potential 1.5 V; (- - -) switching potential 1.3 V.

(Tables 5 and 6). The Ru/Pd complex **1** begins to yield more of the four-electron oxidation product as the reaction progresses, and similar (but more rapid) changes in behavior are observed for Ru/Au complex **2**. In contrast, Ru complex **5** affords only trace amounts of dimethyl acetal under dry conditions. Under wet conditions, **5** favors methyl formate formation, but the reaction is very slow.

During exhaustive bulk electrolysis, oxidative currents gradually decrease to insignificant amounts as the solutions develop a brown discoloration. The lifetimes of the catalysts have not yet been established due to difficulties with our electrolysis cell, in which bulk

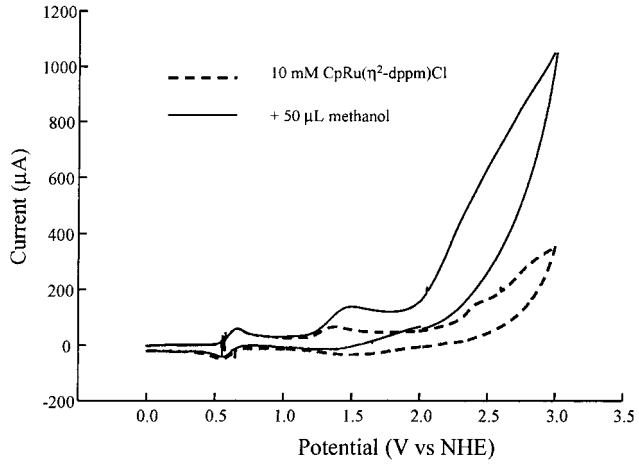

Figure 5. Cyclic voltammogram of **5** under nitrogen in 2.5 mL of DCE/0.7 M TBAT; glassy carbon working electrode; Ag/Ag^+ reference electrode; 50 mV/s.

Table 5. Product Distributions and Current Efficiencies for the Electrochemical Oxidation of Dry Methanol by 1, 2, and 3[a]

	product ratio (μmol of $CH_2(OCH_3)_2$/$HCOOCH_3$)[b]			
charge/(C)	Ru/Pt (**3**)	Ru/Pd (**1**)	Ru/Au (**2**)	Ru (**5**)
25	2.45	3.18	1.44	n.o.[c]
50	2.35	2.41	1.23	n.o.[c]
75	1.51	1.54	0.98	n.o.[c]
100	1.23	0.94	0.59	n.o.[c]
130	1.20	0.87	0.46	∞[d]
efficiency	18.6[e]	24.6[e]	25.4[e]	3.2[f]

[a] Electrolyses were performed at 1.7 V vs NHE. A catalyst concentration of 10 mM was used. Methanol concentration was 0.35 M. [b] Determined by GC with respect to heptane as an internal standard. Each ratio is reported as an average of 2−5 experiments. [c] No products observed. [d] Only $CH_2(OCH_3)_2$ observed. [e] Average current efficiencies after 75−130 C of charge passed. [f] Current efficiency after 130 C of charge passed.

Table 6. Product Distributions and Current Efficiencies for the Electrochemical Oxidation of Wet Methanol by 1, 2, and 3[a]

	product ratio (μmol of $CH_2(OCH_3)_2$/$HCOOCH_3$)[b]			
charge/(C)	Ru/Pt (**3**)	Ru/Pd (**1**)	Ru/Au (**2**)	Ru (**5**)
25	1.68	1.38	1.26	n.o.[c]
50	1.34	0.98	1.05	n.o.[c]
75	1.17	0.84	0.97	n.o.[c]
100	0.67	0.70	0.41	n.o.[c]
130	0.41	0.54	0.34	0.33
efficiency	19.5[d]	20.6[d]	26.1[d]	7.2[e]

[a] Conditions the same as in Table 5 except for the addition of 5 μL of water to the cell. [b] Determined by GC with respect to heptane as an internal standard. Each ratio is reported as an average of 2−5 experiments. [c] No products observed. [d] Average current efficiencies after 75−130 C of charge passed. [e] Current efficiency after 130 C of charge passed.

electrolysis past 130 C is complicated by the diffusion of the catalyst between the compartments. Analysis of the catalyst solutions by ^{31}P NMR after exhaustive bulk electrolysis indicates the decomposition of the original bimetallic structures to complex mixtures of other unidentified phosphorus-containing metal complexes.

Current efficiencies are also summarized in Tables 5 and 6. These values are the ratio of the charge necessary to produce the observed yields of $CH_2(OCH_3)_2$ and $HCOOCH_3$ to the total charge passed during bulk electrolysis. Although the current efficiencies for heterobinuclear complexes **1**−**3** were moderately low (19 to 26%), they are significantly higher than the 3.2 and 7.2% current efficiencies obtained from the mononuclear model compound $CpRuCl(\eta^2$-dppm) (**5**) under dry and wet conditions, respectively. Although the nature of the metal−metal interaction varies in complexes **1**−**3**, in each case the presence of the second metal center apparently results in enhanced catalytic activity.

Summary

We have prepared three Ru-containing heterobinuclear complexes which display catalytic activity toward the electrooxidation of methanol. Our results suggest that cooperativity between metal centers in these well-defined bimetallic systems results in a significant enhancement of current efficiency for the oxidation of methanol. Although the efficiency increase is consistent among the complexes, product ratios of formaldehyde dimethyl acetal to methyl formate vary with the identity of the second metal. Addition of water enhances the oxidative currents and favors the formation of methyl formate in all complexes. Mechanistic studies and further investigations of the nature of the metal−metal interaction during oxidation are currently underway.

Experimental Section

General Considerations. Standard Schlenk/vacuum techniques were used throughout. Hexane, methylene chloride, and 1,2-dichloroethane were distilled from CaH_2. All NMR solvents were degassed via freeze−pump−thaw cycles and stored over molecular sieves. ^1H and ^{31}P NMR spectra are referenced to the residual proton in the deuterated solvent and to 85% H_3PO_4, respectively. The ^{31}P NMR spectra were proton-decoupled. High-resolution mass spectrometry was performed by the University of Florida analytical service. $Cp(PPh_3)RuCl(\eta^1$-dppm) was prepared as previously described.[47] $AuPPh_3Cl$ and $Pd(COD)Cl_2$ were purchased from Strem Chemicals and used as received. $RuCl_3 \cdot xH_2O$ was purchased from Pressure Chemicals. All other starting materials were purchased in reagent grade purity and used without further purification.

Electrochemistry. Electrochemical experiments were performed under nitrogen using an EG&G PAR model 263A potentiostat/galvanostat. Cyclic voltammograms (scan rate of 50 mV/s) were recorded in 2.5−3.5 mL of DCE/0.7 M TBAT at ambient temperature under nitrogen. All potentials are reported vs NHE and referenced to Ag/Ag^+. The reference electrode consisted of a silver wire immersed in an acetonitrile solution containing freshly prepared 0.01 M $AgNO_3$ and 0.1 M TBAT. The Ag^+ solution and silver wire were contained in a 75 mm glass tube fitted at the bottom with a Vycor tip. All electrochemical measurements were performed inside a glovebox. Constant potential electrolysis was performed in a three-compartment H-cell separated by a medium-porosity sintered glass frit in 2.5−3.5 mL of DCE/0.7 M TBAT at room temperature under nitrogen using a vitreous carbon working electrode and platinum foil counter electrode. Cyclic voltammetry was performed with a highly polished glassy-carbon working electrode (3 mm diameter). Electrolysis products were analyzed by gas chromatography on an HP5980A chromatograph containing a 15 m × 0.32 mm column of AT-WAX (Alltech, 0.5 μm film) on fused silica. The column was attached to the injection port with a neutral 5 m × 0.32 mm AT-Wax deactivated guard column. The products produced during electrolysis were quantitatively determined with the use of a

(47) Bruce, M. I.; Humphrey, M. G.; Patrick, J. M.; White, A. H. *Aust. J. Chem.* **1983**, *36*, 2065−2072.

known amount of *n*-heptane as an internal standard. Product identity was confirmed by comparing retention times of the oxidation products with authentic samples.

Cp(PPh$_3$)Ru(μ-Cl)(μ-PPh$_2$CH$_2$PPh$_2$)PdCl$_2$ (1). In a 100 mL flask, Cp(PPh$_3$)RuCl(η^1-dppm) (0.227 g, 0.268 mmol) and PdCl$_2$(COD) (0.077 g, 0.27 mmol) were dissolved in 50 mL of CH_2Cl_2. The red-orange solution was stirred at room temperature for 24 h. The solution was concentrated to a small volume, and hexane was vacuum transferred to precipitate a red solid. The solid was filtered with a swivel medium frit, washed with hexanes, and dried under vacuum. The product was further recrystallized from CH_2Cl_2/hexane to yield 0.195 g (71%) of **1**. Single crystals suitable for X-ray diffraction were grown by slow solvent diffusion of hexane into a solution of the red product in 1,2-dichloroethane. ^{1}H NMR ($CDCl_3$): δ 8.14−6.04 (m, 35H, *Ph*$_2$PCH$_2$P*Ph*$_2$ + P*Ph*$_3$), 4.72 (s, 5H, Cp), 2.71−2.63 (m, 2H, Ph$_2$P*CH*$_2$PPh$_2$). ^{31}P NMR ($CDCl_3$): δ 52.2 (dd, Ru-*P*Ph$_2$-CH$_2$PPh$_2$, J_{PP} = 28 Hz, 35 Hz), 37.5 (d, Ru-*P*Ph$_3$, J_{PP} = 35 Hz), 19.7 (d, PPh$_2$CH$_2$*P*Ph$_2$-Pd, J_{PP} = 28 Hz). HRMS (FAB): calcd for $C_{48}H_{42}Cl_3PdP_3Ru$ 990.0026 (MH^+−Cl), found 990.0073. Anal. Calcd for $C_{48}H_{42}Cl_3PdP_3Ru$: C, 56.21; H, 4.12. Found: C, 55.98; H, 4.00.

Cp(PPh$_3$)RuCl(μ-PPh$_2$CH$_2$PPh$_2$)AuCl (2). The reaction was performed similarly as for **1** starting from CpRu(PPh$_3$)Cl(η^1-dppm) (0.300 g, 0.354 mmol) and PPh$_3$AuCl (0.175 g, 0.354 mmol). Yield: 0.251 g (66%). Single crystals suitable for X-ray diffraction were obtained by recrystallization from CH_2Cl_2/hexane. ^{1}H NMR ($CDCl_3$): δ 7.91−6.83 (m, 35H, *Ph*$_2$PCH$_2$P*Ph*$_2$ + P*Ph*$_3$), 4.74 (m, 1H, Ph$_2$PC*H*HPPh$_2$), 4.09 (s, 5H, Cp), 1.33 (m, 1H, Ph$_2$PCH*H*PPh$_2$). ^{31}P NMR ($CDCl_3$): δ 42.8 (d, Ru-*P*Ph$_3$, J_{PP} = 43 Hz), 36.3 (dd, Ru-*P*Ph$_2$-CH$_2$PPh$_2$, J_{PP} = 28 Hz, 43 Hz), 20.8 (d, Au*P*Ph$_2$CH$_2$PPh$_2$, 28 Hz). HRMS (FAB): calcd for $C_{48}H_{42}Cl_2P_3AuRu$ 1080.0585 (M^+), found 1080.0585. Anal. Calcd for $C_{48}H_{42}Cl_2P_3AuRu$: C, 53.35; H, 3.92. Found: C, 53.62; H, 3.83.

Crystallographic Structure Determination of 1. Data were collected at 173 K on a Siemens SMART PLATFORM equipped with a CCD area detector and a graphite monochromator utilizing Mo Kα radiation (λ = 0.71073 Å). Cell parameters were refined using up to 8192 reflections. A hemisphere of data (1381 frames) was collected using the ω-scan method (0.3° frame width). The first 50 frames were remeasured at the end of data collection to monitor instrument and crystal stability (maximum correction on I was < 1%). Absorption corrections by integration were applied based on measured indexed crystal faces. The structure was solved by the direct methods in SHELXTL5 and refined using full-matrix least squares. The non-H atoms were treated anisotropically, whereas the hydrogen atoms were calculated in ideal positions and were riding on their respective carbon atoms. The C6 protons were refined freely. Three 1,2-dichloroethane molecules of crystallization were found in the asymmetric unit. All three were disordered, and each was refined in two parts. Their site occupation factors were dependently refined to 0.54(1), 0.52(1), and 0.67(1) for the major parts and consequently 0.46(1), 0.48(1) and 0.33(1) for the minor parts. A total of 666 parameters were refined in the final cycle of refinement using 10 952 reflections with $I > 2\sigma(I)$ to yield R_1 and wR_2 of 3.46% and 7.76%, respectively. Refinement was done using F^2. All software and sources of the scattering factors are contained in the SHELXTL program library.[48]

Crystallographic Structure Determination of 2. Data were collected at 173 K on a Siemens SMART PLATFORM equipped with a CCD area detector and a graphite monochromator utilizing Mo Kα radiation (λ = 0.71073 Å). Cell parameters were refined using up to 8192 reflections. A hemisphere of data (1381 frames) was collected using the ω-scan method (0.3° frame width). The first 50 frames were remeasured at the end of data collection to monitor instrument and crystal stability (maximum correction on I was <1%). Absorption corrections by integration were applied based on measured indexed crystal faces. The structures were solved by the direct methods in SHELXTL5 and refined using full-matrix least squares. The asymmetric unit of **2** contained three molecules, the molecule of interest and two CH_2Cl_2 solvent molecules, one of which is located on a center of inversion. Thus, the ratio of complex **2** to solvent is 1:1.5. The non-H atoms were treated anisotropically, whereas the methyl hydrogen atoms were calculated in ideal positions and were riding on their respective carbon atoms. A total of 552 parameters were refined in the final cycle of refinement using 8794 reflections with $I > 2\sigma(I)$ to yield R_1 and wR_2 of 3.84% and 4.26%, respectively. Refinement was done using F^2. All software and sources of the scattering factors are contained in the SHELXTL program library.[48]

Acknowledgment. The Division of Chemical Sciences, Office of Basic Energy Sciences, U.S. Department of Energy, provided funding for this work. K.A.A. wishes to acknowledge the National Science Foundation and the University of Florida for funding of the purchase of the X-ray equipment.

Supporting Information Available: Tables of bond distances, bond angles, positional parameters, and anisotropic displacement parameters for **1** and **2**. This material is available free of charge via the Internet at http://pubs.acs.org.

OM010706H

(48) Sheldrick, G. M. *SHELXTL program library*; Bruker-AXS: Madison, WI, 1998.